npj | clean water

Article

Published in partnership with King Fahd University of Petroleum & Minerals

https://doi.org/10.1038/s41545-024-00397-4

Quantitative Raman analysis of microplastics in water using peak area ratios for concentration determination

Eun Su Jung, Jin Hyun Choe, Jin Seok Kim, Da Won Ahn, JinUk Yoo, Tae Min Choi & Sung Gyu Pyo

This study presents a novel analytical method for the quantitative and qualitative analysis of microplastics (MPs) in deionized (DI) water using Raman spectroscopy. Raman peak area ratios of 1295 cm^{-1} for polyethylene (PE) and 637 cm^{-1} for polyvinylchloride (PVC) to the broad H_2O peak were utilized to establish a calibration model for the concentration of MPs dispersed in DI water at 0.1 wt% to 1.0 wt%. The calibration model demonstrated R^2 values of 0.98537 for PE and 0.99511 for PVC, indicating high linearity between the peak area ratio and concentration. The calibration model was validated using mixed PE and PVC samples to confirm its applicability to real-world water bodies, where multiple types of MPs are present. The calculated standard error of calibration (SEC) and relative standard error of calibration (%RSEC) values further confirmed the accuracy of the predictions, providing a robust approach for detecting and quantifying MPs in aquatic environments.

Microplastics (MPs) were defined by Thompson in 2004 as plastic particles ranging in size from 1 μm to 5 mm[1]. These MP particles originate from plastic products discarded in nature through the continuous disintegration by light or heat or via biodegradation[2]. Since the first report of MPs detected on the sea surface in 1972[3], research has increasingly focused on detecting MPs across a range of aquatic environments, including marine[4], freshwater[5], and river systems[6], as well as aquatic organisms such as zooplankton[7,8] and fish[9]. Over time, this research has expanded to include terrestrial ecosystems[10,11] within the human food chain, along with everyday consumables like tap/drinking water[12], honey, and milk[13]. Recent studies have detected MPs in the digestive[14,15] and respiratory systems[16–18] through ingestion and inhalation. Moreover, the increasing detection of MPs in placenta[19], blood[20], and urine[21], which are not directly related to inhalation or ingestion, has amplified concerns regarding the accumulation of MPs, their circulation within the body, and associated adverse health effects[22].

Water bodies serve as a major source of MPs because they are closely linked to the human food chain and daily life[23,24]. Therefore, numerous analytical techniques are used to detect MPs within water bodies. Current studies on the quantitative and qualitative analysis of MPs in water include optical analysis[25], thermal analysis[26–28], and spectroscopic analysis[29–33]. Optical methods enable rapid, cost-effective analysis through visual sorting and particle counting. However, these methods cannot accurately distinguish between MPs and other particles, such as algae or clay, since identification relies solely on visual distinction[25]. Thermal analysis methods, such as TGA-MS and pyrolysis-GC/MS, thermally degrade the sample and trap the resulting gaseous compounds for mass spectrometric analysis. Qualitative and quantitative analysis are then made by comparing the mass spectra with reference data[26,27]. Majewsky et al. analyzed the concentrations of polyethylene (PE) and polypropylene (PP) in wastewater using TGA-DSC[28]. After pre-determining the calibration curves for 1 mg ~ 20 mg of PE and PP particles, the concentration of PE and PP in the wastewater samples were analyzed by comparing the TGA-DSC peak areas of the samples with those of the calibration curves. While thermal analysis provides highly sensitive and accurate measurements, it is limited to particles larger than 500 μm, and the sample undergoes deformation through heating which prevents further analysis[34].

Among the various techniques used to identify MPs in aqueous sample, vibrational spectroscopy, such as Fourier transform infrared (FT-IR) and Raman spectroscopy, is the most widely employed[29]. It works by exciting and detecting molecular vibrations within a sample, generating unique spectral fingerprints in FT-IR or Raman spectra. These spectra provide specific information about chemical bonding and polymer composition, and are used for both quantitative and qualitative analysis[30]. For FT-IR spectroscopy, the sample is exposed to infrared light within the mid-IR range (400 cm^{-1} ~4000 cm^{-1}). IR absorption requires a change in the dipole moment of a chemical

School of Integrative Engineering, Chung-Ang University, Seoul, Republic of Korea. e-mail: sgpyo@cau.ac.kr

bonds, making it effective for the analysis of polar functional groups. Specific wavelengths of IR radiation are absorbed based on the molecular structure of the sample, and the resulting signal is measured in either transmission or reflection mode[31,32]. Tagg et al. identified five types of MPs – PE, PP, polyethylene terephthalate (PET), polyvinyl chloride (PVC), and polystyrene (PS) – in wastewater using focal plane array (FPA)-based reflectance FT-IR imaging[32]. This technique captured thousands of spectra simultaneously from MPs on the filter paper, offering a comprehensive chemical analysis of the entire surface. FT-IR enables rapid analysis and is unaffected by MP particle size. Moreover, its combination of spectral and imaging capabilities allows for the analysis of large areas, acquiring thousands of spectra in a single measurement[33].

All of the techniques mentioned above are unable to directly analyze liquid samples, making filtration or separation necessary as part of the sample preparation process. In particular, FT-IR is significantly affected by water (H_2O), which is highly IR-active and produces broad peak that cause spectral overlap, hindering analysis and reducing sensitivity[25]. Due to these limitations, this study adopted Raman spectroscopy, which experiences less interference from water, making it more suitable for analyzing aqueous samples.

Raman spectroscopy provides data on molecular vibrations within a material based on the inelastic scattering of photons interacting with the sample[35]. When exposed to monochromatic light (laser), most of the light is elastically scattered at different frequencies, a phenomenon known as Raman scattering. This scattered light generates a spectral fingerprint unique to the molecular composition of the sample[36,37]. Beyond offering quantitative and qualitative information, Raman spectroscopy provides detailed data on particle size, variety, and distribution within a sample, making it widely applicable across various fields[38,39]. Its rapid, non-destructive, along with the low scattering intensity from water molecules that minimally impacts the overall spectrum, has made it useful for detecting MPs in drinking water, sea water, and various other research applications.

Rytelewska et al. analyzed PE from various environmental sites, including riverbanks and forest areas using Raman spectroscopy[40]. They examined the ratio between symmetric and asymmetric -CH_2 stretching bands at 2848 cm^{-1} and 2882 cm^{-1}, to determine crystallinity and density. Also, the appearance of a carbonyl peak at 1643 cm^{-1} indicated oxidative weathering of PE. Additionally, multiple studies have applied Raman spectroscopy to investigate the effects of water quality and hardness, further demonstrating its potential for optical evaluation of water hardness and detection of microplastics in tap and wastewater[41,42].

To analyze the concentration of chemicals, Raman spectroscopy typically examines the intensity or area of specific peaks, with increasing proportionally to the sample concentration. Ma et al. [36] and Moreno et al. [43] utilized Raman peak intensity and area to quantify pharmaceutical mixtures and the concentration of H_2O_2 in CMP slurry. However, quantitative analysis of MPs in water using Raman spectroscopy remains underexplored. Additionally, since peak intensities fluctuate depending on measurement conditions, it allows for relative comparison between samples but does not provide absolute concentration values.

In this study, a novel method is proposed to predict the concentration of MPs in aqueous samples using Raman spectroscopy by introducing the area ratio between the characteristic peaks of MPs and the water peak. Calibration data, set as the predicted values, were developed by analyzing PE and PVC samples at various concentrations. The calibration model was then validated by comparing the predicted values with the true concentrations of mixture of PE and PVC solutions. These findings are expected to enable precise real-time monitoring and analysis of MPs in various water bodies such as seawater and drinking water, providing a benchmark for accurate concentration measurements.

Methods

Preparation of MP samples

In this study, concentration-based detection of polyethylene (PE) and polyvinyl chloride (PVC) was conducted. Both PE and PVC were composed of spherical white particles, with PE particle sizes ranging from 40 μm ~ 48 μm and PVC particle sizes ranging from 40 μm ~ 100 μm. Both materials were purchased from Sigma-Aldrich.

Figure 1 shows the samples used for calibration model (Fig. 1a) and the true concentration (Fig. 1b). For calibration purposes, separate sample of PE with deionized (DI) water and PVC with DI water were prepared at varying concentrations (0.1 wt% ~ 1.0 wt%). To determine the true value, PE, PVC, and DI water were mixed together at the sample concentration range (0.1 wt% ~ 1.0 wt%). The concentration (wt%) of each sample was adjusted to 10 mL of DI water (density of DI water set to 1.0) based on the weight. Since PE and PVC particles are not soluble, the mixtures were stirred at 600 rpm for 30 minutes at room temperature to ensure dispersion.

Raman measurement

Raman spectra of MP samples were obtained using a confocal Raman spectrometer (XperRam C series, Nanobase Inc., Korea). A 5 X magnification lens and a 30 mW, 532 nm laser were used to irradiate the sample, with a scanning area of 800 × 800 μm. Each spectrum was collected with a measurement time of 25 s, and 20 spectra were analyzed per sample. For linear plotting, each data point was generated by averaging the 20 measured spectra using the Gaussian method. Figure 2 provides a schematic illustration of the confocal Raman spectroscopy detecting MP samples.

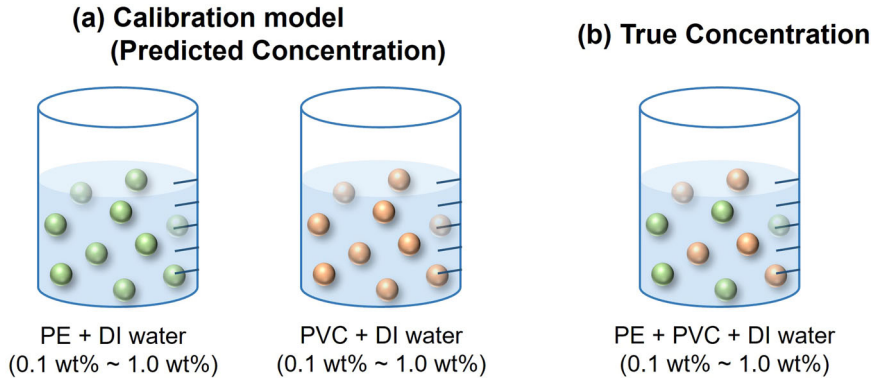

Fig. 1 | Schematic illustration of calibration and true concentration samples. a Sample used for calibration (predicted) data; PE particles and PVC particles are each mixed with DI water at concentrations ranging from 0.1 wt% to 1.0 wt%. **b** Sample used for true concentration data; both PE and PVC particles are mixed together in DI water at concentrations ranging from 0.1 wt% to 1.0 wt%.

Data analysis

For the calibration of concentration analysis using peak area ratios, solutions of PE and PVC were prepared in concentrations ranging from 0.1 wt% to 1.0 wt% and analyzed via Raman spectroscopy. Table 1 presents the properties of PVC and PE used in this study, along with the Raman peak information obtained using 532 nm excitation[44,45]. The bolded peaks are the ones used to identify the two substances in the Raman spectrum of the PE and PVC mixture sample for validation (Fig. 5). The most intense peaks, at 1295 cm^{-1} for PE and 637 cm^{-1} for PVC, along with the peak area ratio relative to H_2O, were plotted. These data were then subjected to linear fitting using the Origin software (Fig. 4). The results of the linear fitting were expressed in terms of the slope, intercept, and the coefficient of determination (R^2), which represents the proportion of variance in the dependent variable that can be explained by the independent variables (Eq. 1)[46]. In Equation 1, X_i denotes the peak area ratio obtained from the analysis, while Y_i represents the reference data derived from the linear fitted graph. The variable n represents the number of data points analyzed.

$$R^2 = 1 - \frac{\sum_{i=1}^{n}(X_i - Y_i)^2}{\sum_{i=1}^{n}(Y - Y_i)^2} \quad (1)$$

The validation of the calibration data was conducted by comparing the detection results of PE and PVC in the mixture, with the true concentration and calibration data as the predicted values. The prediction ability was evaluated using the standard error of calibration (SEC) (Eq. 2) and the relative standard error of calibration (RSEC%) (Eq. 3)[46]. SEC quantifies the average deviation between the predicted values from the calibration model and the true values. A lower SEC value indicates a better fit of the calibration model, meaning that the predicted values closely align with the true data. This metric reflects the model's effectiveness in predicting concentrations within the calibration dataset. RSEC% expresses the SEC as a percentage of the mean true concentration, providing a relative measure of the error. This allows for a comparison of the calibration error across concentration ranges. A lower RSEC% indicates higher accuracy in predicting concentrations relative to the magnitude of the true values. The variable n represents the number of samples. C_{Raman} corresponds to the peak area ratio obtained from the true concentration, while C_{Ref} represents the predicted data derived from the calibration.

$$SEC = \sqrt{\frac{\sum_{i=1}^{n}\left(C_{RAMAN\,i} - C_{REF_i}\right)^2}{n}} \quad (2)$$

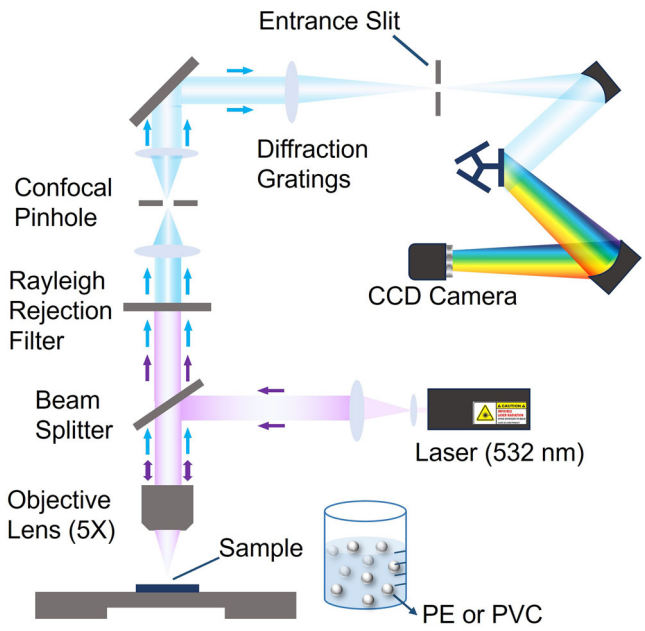

Fig. 2 | Schematic diagram of confocal Raman spectroscopy. The following schematic illustrates the operating principle of the confocal Raman spectroscopy used in this study.

Table 1 | Polymer sample properties and Raman peaks of each polymer

Polymer	Size	Shape (Color)	Raman peaks (cm^{-1})
Polyvinyl chloride (PVC)	40 ~ 100 μm	Sphere (White)	310, 345, **363**, 420, 496, 544, 571, 599, 615, **637**, 682, **694**, 752, 838, 930, 964, 972, 1066, 1101, 1119, 1172, 1187, 1216, 1257, 1316, 1335, 1379, **1430**, 1437, 1498, 2914, 2935, 2969, 2994
Polyethylene (PE)	40 ~ 48 μm	Sphere (White)	**1062, 1129**, 1170, **1295**, 1417, 1440, 1460, 2850, 2883

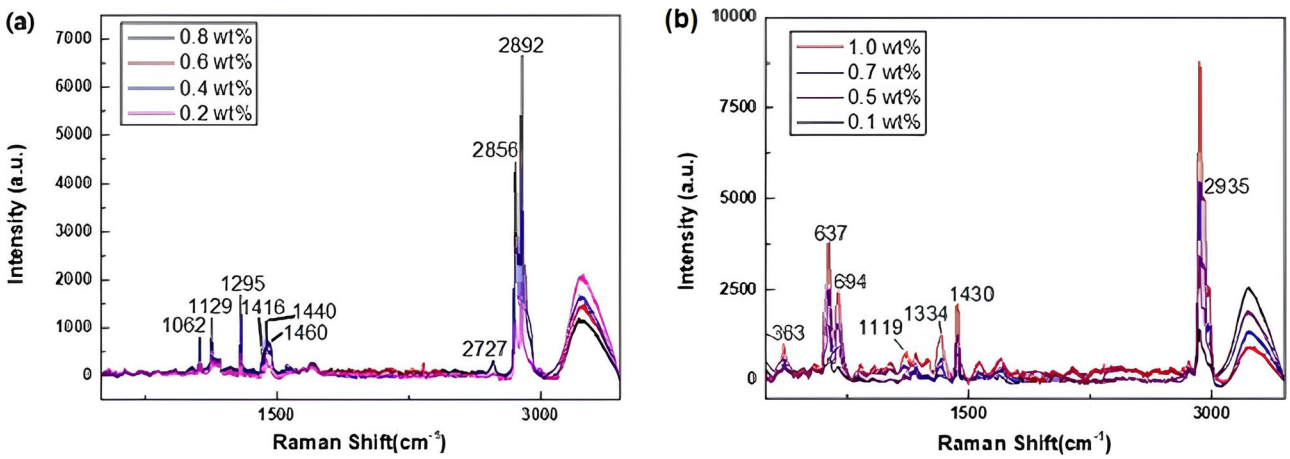

Fig. 3 | Raman spectra analysis of PE and PVC at varying concentrations for calibration. Raman spectra of **a** PE, **b** PVC particles in DI water at different concentrations (0.2, 0.4, 0.6, and 0.8 wt%).

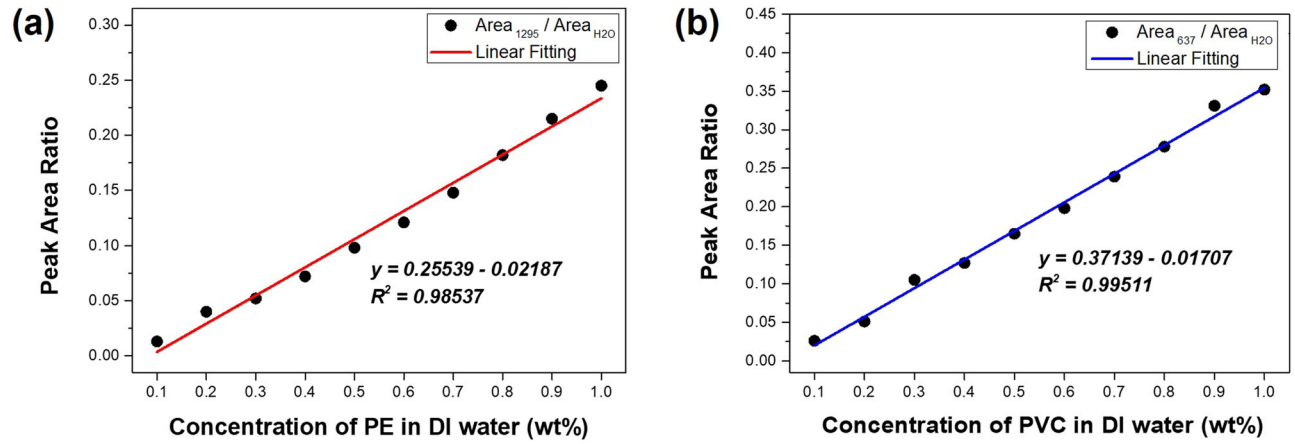

Fig. 4 | Calibration model of PE and PVC based on peak area ratios. Calibration model of **a** PE plotted by peak area ratio ($Area_{1295}/Area_{H2O}$) and **b** PVC plotted by peak area ratio ($Area_{637}/Area_{H2O}$).

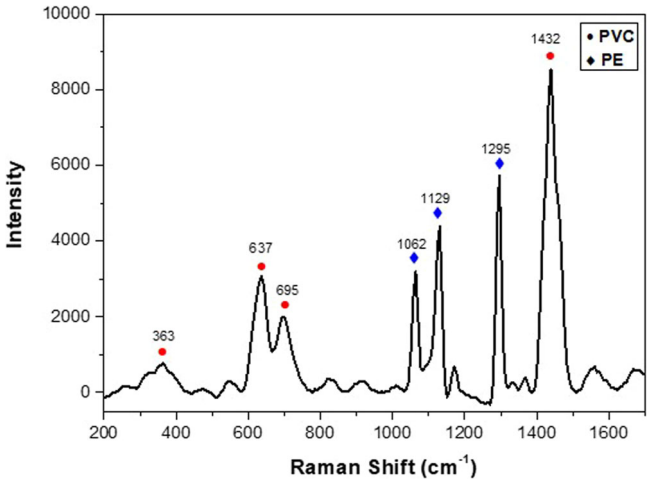

Fig. 5 | Raman spectrum of PE and PVC at 1.0 wt% for validation. Raman spectrum of mixture of PE 1.0 wt% and PVC 1.0 wt% with DI water. In the Raman spectrum of the mixture, the Raman bands of PE at 363 cm^{-1}, 637 cm^{-1}, 695 cm^{-1}, and 1432 cm^{-1}, as well as the Raman bands of PVC at 1062 cm^{-1}, 1129 cm^{-1}, and 1295 cm^{-1}, were all observed.

$$\%\mathrm{RSEC} = \sqrt{\frac{\sum_{i=1}^{n}\left(C_{\mathrm{RAMAN}_i} - C_{\mathrm{REF}_i}\right)^2}{\sum_{i=1}^{n} C_{\mathrm{REF}_i}^2}} \times 100 \quad (3)$$

Quality assurance (QA)/quality control (QC)

Prior to preparing samples by mixing PE and PVC particles, Raman analysis of deionized water confirmed the absence of MP fibers and particles. All laboratory equipment used in the sample preparation process was made of glass, ensuring no contamination from plastic materials.

Result and discussion

Quantitative and qualitative analysis of MP by Raman spectroscopy

Figure 3 shows the plotted Raman spectra for MP solution samples at various concentrations. Figure 3a shows the Raman peaks for PE and Fig. 3b for PVC, with each figure demonstrating that the intensity of the peaks increases as the concentration rises.

Figure 3a shows the Raman spectra of the samples with different concentrations of PE particles in deionized water. The Raman peaks of the PE particles appeared at 1062 cm^{-1}, 1129 cm^{-1}, 1295 cm^{-1}, 1416 cm^{-1}, 1440 cm^{-1}, 1460 cm^{-1}, 2727 cm^{-1}, 2856 cm^{-1}, and 2892 cm^{-1}. 1062 cm^{-1} and 1129 cm^{-1} correspond to the asymmetric and symmetric stretching vibrations of the C–C bond, respectively. 1295 cm^{-1} and 1416 cm^{-1} peaks correspond to the twisting and wagging vibrations of the CH_2 bond, respectively. The peaks between 1400 cm^{-1} and 1440 cm^{-1} correspond to the overtones of the CH_2 bonds. The peaks at 2856 cm^{-1} and 2892 cm^{-1} correspond to the symmetric and asymmetric stretching vibrations of the CH_2 group, respectively[28]. The broad peak around 3400 cm^{-1} is attributed to the OH stretching of H_2O.

Figure 3b represents the Raman spectra for the PVC particles at different concentrations in deionized water. The PVC peaks appear at 363 cm^{-1}, 637 cm^{-1}, 694 cm^{-1}, 1119 cm^{-1}, 1334 cm^{-1}, 1430 cm^{-1} and 2935 cm^{-1}. The 637 cm^{-1} and 694 cm^{-1} peaks correspond to the stretching vibrations of the C–Cl bond. The peaks at 363 cm^{-1}, 1119 cm^{-1}, 1334 cm^{-1}, 1430 cm^{-1}, and 2935 cm^{-1} also correspond to PVC[47].

Figure 4 shows the result of the calibration model as an internal standard. The data were plotted based on the area ratio values of the 1295 cm^{-1} peak of PE and the 637 cm^{-1} peak of PVC to the H_2O peak. These values were then linearly fitted to generate the calibration graphs. Figure 4a presents the calibration model for PE, resulting in a linear equation of y = 0.25539–0.02187 with an R^2 = 0.98537, while Fig. 4b shows the PVC calibration model with a linear equation of y = 0.37139–0.01717 with an R^2 = 0.99511.

Validation of data

To validate the calibration model, PE and PVC were mixed with DI water at concentrations ranging from 0.1 wt% to 1.0 wt%, and the resulting samples were analyzed using Raman spectroscopy. The results were ten compared with the calibration model. Figure 5 illustrates the Raman spectrum of a mixture sample containing 1.0 wt% PE and 1.0 wt% PVC. Peaks for both PE and PVC were detected within the same spectrum, and these peaks were marked as the bolded peaks in Table 1.

The area ratio values of the intense peaks selected for calibration and the H_2O peak were plotted on the linear fitting results of the calibration model in Fig. 6. Figure 6a shows the result of plotting the true values of the 1295 cm^{-1} (PE) and H_2O peak area ratio from Fig. 5 on the red linear graph representing the calibration data. The SEC for this result is 0.07232114 and the %RSEC is 0.48052 (Table 2). Figure 6b shows the result of plotting the 637 cm^{-1} (PVC) and H_2O peak area ratio from Fig. 5 onto the blue linear graph. The SEC and %RSEC data from Table 2 are 0.0985576 and 0.52645, respectively. The SEC and %

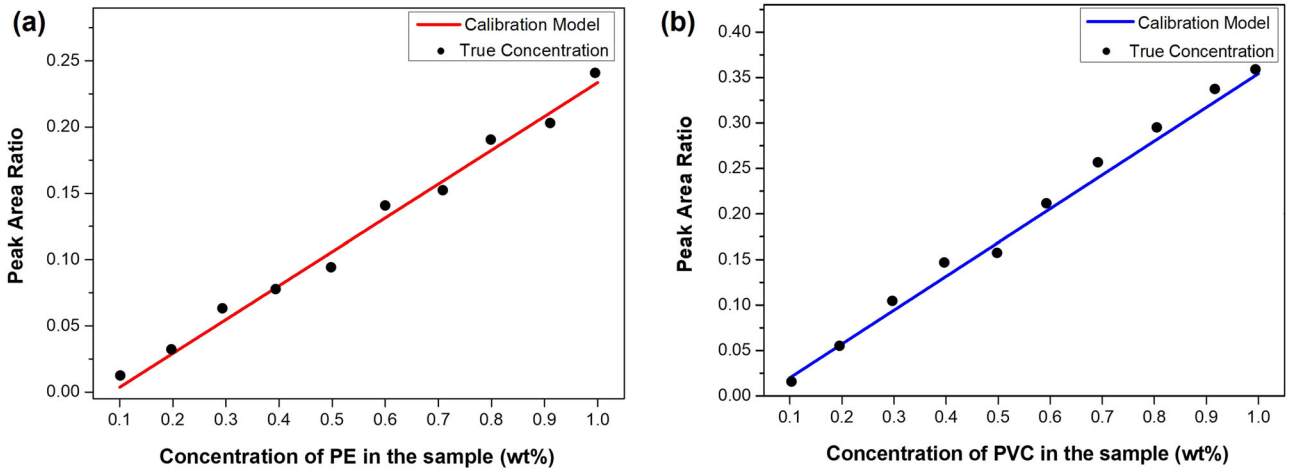

Fig. 6 | Validation results by plotting true data with calibration data (predicted values). Linear plot of the calibration data was created as shown in Fig. 4, **a** red graph for PE and **b** blue graph for PVC, with the true value results overlaid as dotted data points.

Table 2 | Prediction results of polyethylene (PE) and polyvinyl chloride (PVC) in DI water

Component	SEC	%RSEC
Polyethylene (PE)	0.0723214	0.48052
Polyvinyl chloride (PVC)	0.0985576	0.52645

RSEC values for PE and PVC align closely with the calibration data and true concentration results, demonstrating the validity of the method proposed in this study.

Data availability

All data are available upon request.

Received: 31 July 2024; Accepted: 25 September 2024;
Published online: 09 October 2024

References

1. Thompson, R. C. et al. Lost at sea: where is all the plastic? *Science* **304**, 838–838 (2004).
2. Cózar, A. et al. Plastic debris in the open ocean. *Proc. Natl. Acad. Sci. USA* **111**, 10239–10244 (2014).
3. Carpenter, E. J. & Smith, K. L. Plastics on the Sargasso sea surface. *Science* **175**, 1240–1241 (1972).
4. Ram, B. & Kumar, M. Correlation appraisal of antibiotic resistance with fecal, metal and microplastic contamination in a tropical Indian river, lakes and sewage. *NPJ Clean. Water* **3**, 3 (2020).
5. Lee, E.-H., Lee, S., Chang, Y. & Lee, S.-W. Simple screening of microplastics in bottled waters and environmental freshwaters using a novel fluorophore. *Chemosphere* **285**, 131406 (2021).
6. Strokal, M. et al. River export of macro- and microplastics to seas by sources worldwide. *Nat. Commun.* **14**, 4842 (2023).
7. Kvale, K., Prowe, A. E. F., Chien, C. T., Landolfi, A. & Oschlies, A. Zooplankton grazing of microplastic can accelerate global loss of ocean oxygen. *Nat. Commun*. **12**, https://doi.org/10.1038/s41467-021-22554-w (2021).
8. Richon, C., Gorgues, T., Paul-Pont, I. & Maes, C. Zooplankton exposure to microplastics at global scale: Influence of vertical distribution and seasonality. *Front. Mar. Sci.* **9**, 947309 (2022).
9. Thiele, C. J., Hudson, M. D., Russell, A. E., Saluveer, M. & Sidaoui-Haddad, G. Microplastics in fish and fishmeal: an emerging environmental challenge? *Sci. Rep.* **11**, 2045 (2021).
10. Surendran, U., Jayakumar, M., Raja, P., Gopinath, G. & Chellam, P. V. Microplastics in terrestrial ecosystem: Sources and migration in soil environment. *Chemosphere* **318**, 137946 (2023).
11. Rillig, M. C. & Lehmann, A. Microplastic in terrestrial ecosystems. *Science* **368**, 1430–1431 (2020).
12. Cserbik, D. et al. Human exposure to per- and polyfluoroalkyl substances and other emerging contaminants in drinking water. *NPJ Clean. Water* **6**, 10 (2023).
13. Diaz-Basantes, M. F., Conesa, J. A. & Fullana, A. Microplastics in honey, beer, milk and refreshments in Ecuador as emerging contaminants. *Sustainability* **12**, 5514 (2020).
14. Zhang, Y. et al. The potential effects of microplastic pollution on human digestive tract cells. *Chemosphere* **291**, 132714 (2022).
15. Fournier, E. et al. Microplastics in the human digestive environment: a focus on the potential and challenges facing in vitro gut model development. *J. Hazard. Mater.* **415**, 125632 (2021).
16. Vattanasit, U., Kongpran, J. & Ikeda, A. Airborne microplastics: a narrative review of potential effects on the human respiratory system. *Sci. Total Environ*. **904**, 166745 (2023).
17. Lu, K. et al. Microplastics, potential threat to patients with lung diseases. *Front. Toxicol*. **4**. https://doi.org/10.3389/ftox.2022.958414 (2022).
18. Jeon, M. S. et al. Polystyrene microplastic particles induce autophagic cell death in BEAS-2B human bronchial epithelial cells. *Environ. Toxicol.* **38**, 359–367 (2023).
19. Ragusa, A. et al. Plasticenta: first evidence of microplastics in human placenta. *Environ. Int*. **146**. https://doi.org/10.1016/j.envint.2020.106274 (2021).
20. Leslie, H. A. et al. Discovery and quantification of plastic particle pollution in human blood. *Environ. Int*. **163** https://doi.org/10.1016/j.envint.2022.107199 (2022).
21. Pironti, C. et al. First evidence of microplastics in human urine, a preliminary study of intake in the human body. *Toxics* **11**, 40 (2022).
22. Prata, J. C. Microplastics and human health: integrating pharmacokinetics. *Crit. Rev. Environ. Sci. Technol.* **53**, 1489–1511 (2023).
23. Chakraborty, I. et al. Raman spectroscopy for microplastic detection in water sources: a systematic review. *Int. J. Environ. Sci. Technol.* **20**, 10435–10448 (2023).
24. Niu, J. Q., Xu, D. Y., Wu, W. Q. & Gao, B. Tracing microplastic sources in urban water bodies combining their diversity, fragmentation and stability. *NPJ Clean Water* **7**. https://doi.org/10.1038/s41545-024-00329-2 (2024).

25. Li, J. Y., Liu, H. H. & Chen, J. P. Microplastics in freshwater systems: a review on occurrence, environmental effects, and methods for microplastics detection. *Water Res.* **137**, 362–374 (2018).
26. Forbes, T. P., Pettibone, J. M., Windsor, E., Conny, J. M. & Fletcher, R. A. Rapid chemical screening of microplastics and nanoplastics by thermal desorption and pyrolysis mass spectrometry with unsupervised fuzzy clustering. *Anal. Chem.* **95**, 12373–12382 (2023).
27. Dümichen, E. et al. Analysis of polyethylene microplastics in environmental samples, using a thermal decomposition method. *Water Res.* **85**, 451–457 (2015).
28. Majewsky, M., Bitter, H., Eiche, E. & Horn, H. Determination of microplastic polyethylene (PE) and polypropylene (PP) in environmental samples using thermal analysis (TGA-DSC). *Sci. Total Environ.* **568**, 507–511 (2016).
29. Nguyen, M. K. et al. Microplastics in sewage sludge: distribution, toxicity, identification methods, and engineered technologies. *Chemosphere* **308**, 136455 (2022).
30. Choi, E., Choi, Y., Lee, H., Kim, J. W. & Oh, H. B. Development of a machine-learning model for microplastic analysis in an FT-IR microscopy image. *Bull. Korean Chem. Soc.* **45**, 472–481 (2024).
31. Käppler, A. et al. Analysis of environmental microplastics by vibrational microspectroscopy: FTIR, Raman or both? *Anal. Bioanal. Chem.* **408**, 8377–8391 (2016).
32. Tagg, A. S., Sapp, M., Harrison, J. P. & Ojeda, J. J. Identification and quantification of microplastics in wastewater using focal plane array-based reflectance micro-FT-IR imaging. *Anal. Chem.* **87**, 6032–6040 (2015).
33. Petkovsek, M., Krzan, A., Smid, A., Zagar, E. & Zupanc, M. Degradation of water soluble poly(vinyl alcohol) with acoustic and hydrodynamic cavitation: laying foundations for microplastics. *NPJ Clean Water* **6**. https://doi.org/10.1038/s41545-023-00248-8 (2023).
34. Sorolla-Rosario, D., Llorca-Porcel, J., Pérez-Martínez, M., Lozano-Castelló, D. & Bueno-López, A. Microplastics' analysis in water: Easy handling of samples by a new Thermal Extraction Desorption-Gas Chromatography-Mass Spectrometry (TED-GC/MS) methodology. *Talanta* **253**, 123829 (2023).
35. Kim, J. B. et al. Raman scattering monitoring of thin film materials for atomic layer etching/deposition in the nano-semiconductor process integration. *Chem. Phys. Rev*. **4**. https://doi.org/10.1063/5.0147685 (2023).
36. Ma, X. et al. Raman spectroscopy for pharmaceutical quantitative analysis by low-rank estimation. *Front. Chem.* **6**, 400 (2018).
37. Zou, S. et al. Ag nanorods-based surface-enhanced Raman scattering: synthesis, quantitative analysis strategies, and applications. *Front. Chem*. **7**, 376 (2019).
38. Chen, Q. et al. A review of recent progress in the application of Raman spectroscopy and SERS detection of microplastics and derivatives. *Microchim. Acta* **190**. https://doi.org/10.1007/s00604-023-06044-y (2023).
39. Sridhar, A., Kannan, D., Kapoor, A. & Prabhakar, S. Extraction and detection methods of microplastics in food and marine systems: a critical review. *Chemosphere* **286**, 131653 (2022).
40. Rytelewska, S. & Dąbrowska, A. The Raman spectroscopy approach to different freshwater microplastics and quantitative characterization of polyethylene aged in the environment. *Microplastics* **1**, 263–281 (2022).
41. Li, Z., Wang, J. & Li, D. Applications of Raman spectroscopy in detection of water quality. *Appl. Spectrosc. Rev.* **51**, 313–337 (2016).
42. Ahmed, M., Namboodiri, V., Singh, A. K., Mondal, J. A. & Sarkar, S. K. How ions affect the structure of water: a combined Raman spectroscopy and multivariate curve resolution study. *J. Phys. Chem. B* **117**, 16479–16485 (2013).
43. Moreno, T. et al. Quantitative Raman determination of hydrogen peroxide using the solvent as internal standard: Online application in the direct synthesis of hydrogen peroxide. *Chem. Eng. J.* **166**, 1061–1065 (2011).
44. Jin, Y. et al. Raman identification of multiple melting peaks of polyethylene. *Macromolecules* **50**, 6174–6183 (2017).
45. Nava, V., Frezzotti, M. L. & Leoni, B. Raman spectroscopy for the analysis of microplastics in aquatic systems. *Appl. Spectrosc.* **75**, 1341–1357 (2021).
46. Chicco, D., Warrens, M. J. & Jurman, G. The coefficient of determination R-squared is more informative than SMAPE, MAE, MAPE, MSE and RMSE in regression analysis evaluation. *Peerj Comput. Sci.* **7**, e623 (2021).
47. Luo, Y. et al. Raman imaging of microplastics and nanoplastics generated by cutting PVC pipe. *Environ. Pollut.* **298**, 118857 (2022).

Acknowledgements

This work was supported by the Ministry of Education, Science and Technology (NRF) under Grant NRF-2022R1F1A1063561; the Ministry of Trade, Industry and Energy (MOTIE, Korea) under Grant No. 20022472; the Ministry of Trade, Industry & Energy (MOTIE, Korea) under Grant RS-2023-00237003; and the Ministry of Trade, Industry & Energy (MOTIE, Korea) under Grant 1415187674.

Author contributions

Eun Su Jung: writing - original draft, data curation, investigation, conceptualization. Jin Hyun Choe: data curation, investigation. Jin Seok Kim, Da Won Ahn: methodology. JinUk Yoo, Tae Min Choi: investigation. Sung Gyu Pyo: conceptualization, supervision, writing - review & editing.

Competing interests

The authors declare no competing interests.

Additional information

Correspondence and requests for materials should be addressed to Sung Gyu Pyo.